Atmósfera 39, 525-541 (2025)
https://doi.org/10.20937/ATM.53456

Physical processes of fog in the Brazilian Northeast: Forecast by PAFOG and FogVIS models

Davidson LIMA DE MELO[1,2]*, Augusto G. C. PEREIRA[1], Paulo Vitor DE ALBUQUERQUE MENDES[2], Natalia FEDOROVA[2] and Vladimir LEVIT[2]

[1] *Centro de Previsão do Tempo e Estudos Climáticos, Instituto Nacional de Pesquisas Espaciais, Cachoeira Paulista, 12630-000, São Paulo, Brazil.*
[2] *Instituto de Ciências Atmosféricas, Universidade Federal de Alagoas, Maceió, 57072-970, Alagoas, Brazil.*
*Corresponding author; email: davidson.melo@inpe.br

Received: November 4, 2024; Accepted: May 17, 2025

RESUMEN

No se ha desarrollado un modelo específico para la previsión de baja visibilidad en el Nordeste de Brasil (BNE, por su sigla en inglés), por lo que el modelo parametrizado de niebla (PAFOG), desarrollado en Alemania, fue adaptado para la región. Además, se desarrolló una herramienta para determinar la visibilización de la niebla (FogVIS), basada en ecuaciones simples, que requiere más pruebas. Se recopilaron datos de superficie de reportes meteorológicos de aeródromo y de pronósticos de área terminal de 2008 a 2020, a través de la interfaz de programación de aplicaciones de la Red de Meteorología de la Fuerza Aérea Brasileña, identificando 218 eventos de niebla en tres aeropuertos: Maceió (32 eventos), Recife (un evento) y Campina Grande (185 eventos). Se obtuvieron imágenes satelitales GOES de la base de datos del Centro de Previsión Meteorológica y Estudios del Clima, y se realizaron análisis sinópticos y termodinámicos utilizando los datos de reanálisis ERA5. La humedad de las fuentes de agua cercanas (laguna de Maceió y embalse de Campina Grande) fue un factor determinante en la formación de niebla. El modelo PAFOG mostró un buen rendimiento predictivo para Maceió y el único evento breve de Recife, especialmente en las previsiones a 12 h, particularmente cuando los eventos de niebla fueron precedidos o seguidos por niebla ligera o lluvia. En contraste, la herramienta FogVIS a menudo se alineó estrechamente con el rango de visibilidad observado y proporcionó resultados complementarios 18 h antes para los eventos de Campiña Grande, que fueron más intensos pero estuvieron menos asociados con lluvia o niebla, y también mostró resultados más altos para el Índice de Estabilidad de Niebla. Ambos modelos mostraron eficiencia, destacando el rendimiento de PAFOG en Maceió y FogVIS en Campina Grande, lo que resalta la aplicabilidad y precisión de ambos modelos en la predicción de niebla para el BNE.

ABSTRACT

A specific model for low-visibility forecasting in the Brazilian Northeast (BNE) has not been developed; therefore, the German Parameterized Fog (PAFOG) model was adapted for the region. Additionally, Fog Visibility (FogVIS), a simple equation-based tool, was developed and requires further testing. From 2008 to 2020, Meteorological Aerodrome Report and Terminal Aerodrome Forecast surface data were collected via the Meteorology Network of the Brazilian Air Force Application Programming Interface, identifying 218 fog events across three airports: Maceió (32 events), Recife (1 event), and Campina Grande (185 events). GOES satellite images were accessed from the Center for Weather Forecasting and Climate Studies database, and synoptic and thermodynamic analyses were performed using ERA5 reanalysis data. Humidity from nearby water sources (lagoon for Maceió, dam for Campina Grande) was a primary factor in fog formation. PAFOG demonstrated strong predictive performance for Maceió and Recife's single brief events, especially in 12-h forecasts, particularly when fog events were preceded or followed by mist or light rain. In contrast, FogVIS

often aligned closely with the observed visibility range and provided complementary results 18 hours in advance for Campina Grande's events, which were more intense but less associated with rain or mist, and also showed higher Fog Stability Index results. Both models demonstrated efficiency, with PAFOG excelling in Maceió and FogVIS in Campina Grande, highlighting the applicability and accuracy of both models in predicting fog for the BNE.

Keywords: visibility prediction, airport, statistical evaluation, adverse phenomena.

1. Introduction

Fog, consisting of water droplets suspended near the surface, reduces horizontal visibility to less than 1 km and is a significant factor in aviation, causing delays, cancellations, and accidents (Varejao, 2006; Gultepe et al., 2006). Climatological studies reveal fog is influenced by seasonal and regional factors, with more frequent occurrences in fall and winter near coastlines, driven by synoptic-scale conditions (Akimoto and Kusaka, 2015). Fog development is influenced by temperature, humidity, condensation nuclei, radiative cooling, and the mixing of air masses, with dissipation facilitated by morning temperature increases and turbulence from evapotranspiration (Cotton and Anthes, 1989; França et al., 2019).

In tropical and semi-arid regions such as Brazil's northeastern coast, the climate exhibits seasonal variability, with tropical areas having distinct wet and dry seasons and semi-arid regions experiencing irregular rainfall (Molion and Bernardo, 2002). The periphery of synoptic systems, including troughs in trade winds, often influences fog formation, as low-level moisture convergence interacts with sinking air associated with the jet stream (Fedorova et al., 2015). Key mechanisms for fog formation include coastal moisture sources, low-level confluence, and pre-event precipitation (Fedorova et al., 2016).

Fog forecasting in the Brazilian Northeast (BNE) remains underdeveloped. The Parameterized Fog (PAFOG) model, adapted from Germany, shows potential in predicting fog at Maceio International Airport (Fedorova et al., 2015), while the Fog Visibility (FogVIS) tool, developed at the Universidade Federal de Alagoas (Federal University of Alagoas), forecasts visibility with 24-h lead times and requires further validation for BNE conditions (Nobre et al., 2019). This study aims to analyze fog events over 13 years across three tropical BNE airports, examining their formation, dissipation, synoptic conditions, and forecasts from PAFOG and FogVIS to enhance predictive accuracy for the region.

2. Experiments

The region under study for the presence of fog-causing systems is the BNE (Fig. 1a) over 13 years, from 2008 to 2020, focusing on the airports of Maceió, Alagoas (AL) (9.5º S, 35.8º W, altitude 118 masl), Recife, Pernambuco (PE) (8.1º S, 34.9º W, altitude 4 masl), and Campina Grande, PE (7.3º S, 35.9º W, altitude 502 masl) (Fig. 1b).

Previous studies on fog and low visibility in the BNE have been conducted (Melo et al., 2023), although with varying models and covering only the 2003-2009 period. Despite their low occurrence, fog events in this region remain under-researched and continue to disrupt airport operations unexpectedly, particularly during nighttime.

2.1 Surface data and methodology

A table was prepared detailing fog events occurring at the following airports: (a) Maceió International Airport Zumbi dos Palmares (SBMO); (b) Recife International Airport Gilberto Freyre (SBRF), and (c) Campina Grande International Airport Presidente João Suassuna (SBKG). Data were obtained through the Meteorological Aerodrome Report (METAR) code, collected via the Application Programming Interface (API) of the Rede de Meteorologia do Comando da Aeronáutica (Air Force Meteorology Network; REDEMET). These codes contain information on: (a) pressure (hPa); (b) wind speed (knots); (c) relative humidity (%), and (d) air temperature and dew point (ºC) for the surface, recorded on all days and times when fog (identified as "FG") occurred.

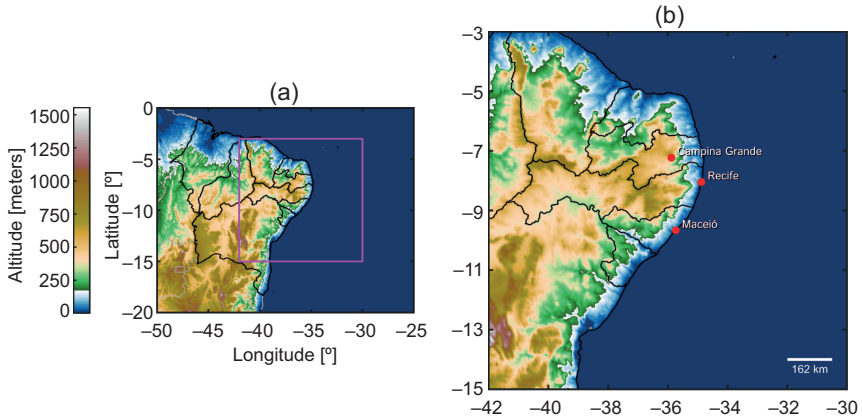

Fig. 1. Study region. (a) Synoptic systems. (b) Cities of fog analysis. Source: Brazilian Institute of Geography and Statistics (IBGE), MATLAB.

Since the METAR code does not directly provide relative humidity, this was derived from the observed temperature and dew point temperature using a simplified equation. This equation estimates the dew point temperature based on the observed air temperature and the relative humidity. Using this relationship, relative humidity was calculated for each fog event, providing an approximation of the humidity conditions during the occurrence of fog. The formula used for this calculation, which has proven to be accurate for relative humidity values above 50%, was proposed by Lawrence (2005):

$$T_d = T - \left(\frac{100 - RH}{5}\right) \quad (1)$$

where T_d is the dew point temperature (in ºC), T is the observed temperature (in ºC), and RH is the relative humidity (in %).

Fog events were selected according to the Instituto de Controle do Espaço Aéreo (Institute of Airspace Control, ICEA) definition, characterized by horizontal visibility ≤ 1000 m and relative humidity above 90%. Events were considered continuous; if fog dissipated, the next occurrence was treated as a new event.

2.2 Satellite images

Images from the GOES-13 satellite were collected on the Centro de Previsão de Tempo e Estudos Climáticos (Center for Weather Forecasting and Climate Studies; CPTEC) platform in the infrared and water vapor channels. These images were used to aid in identifying cloudiness and synoptic-scale systems associated with fog formation at airports.

It is necessary to identify the atmospheric conditions to determine whether the formation of fogs was attributed to radiation or advection. This distinction is essential for assessing the applicability of the PAFOG model, which performs better for radiation fog types. During the investigated period, no cases were observed where both radiation and advection processes occurred simultaneously in the formation of fog.

2.3 Synoptic and thermodynamic analysis

The data files containing meteorological variables were extracted from the ERA5-ECMWF Reanalysis model, with a resolution of 0.25º × 0.25º. These data were used to create synoptic and thermodynamic meteorological fields using the Grid Analysis and Display System (GrADS) graphical tool software.

Standard pressure levels were applied to all recorded phenomena that reduced horizontal visibility at the selected airports. This approach aimed to investigate the tropospheric structure and the primary synoptic systems contributing to fog formation over these airports.

The zonal and meridional components (u and v, in m s^{-1}) of the wind were utilized to generate streamline fields. Additionally, these variables, along with air temperature (T, in K) and relative humidity (RH, in %), were employed to construct vertical profiles in the thermodynamic diagram (Skew-T Log-P). This

analysis aimed to investigate the thermodynamic processes associated with fog formation and mist dampness.

2.4 Forecast by the PAFOG model

The PAFOG model, developed and provided by Prof. Dr. Andreas Bott (Bott and Trautmann, 2002) through an international collaboration with the University of Bonn, Germany, is designed to forecast radiation fog and stratiform clouds in extratropical regions. However, for optimal performance in the BNE, specific adjustments are required.

The PAFOG model operates using a sophisticated parameterization scheme, incorporating a series of prediction equations within its dynamic module (Nickerson et al., 1986; Chaumerliac et al., 1987). Central to this scheme is Eq. (2), which calculates the concentration of total cloud droplets (N_C, in cm^{-3}) and the total water content in the cloud ($_C$).

$$dN_c = \frac{N_c}{\sqrt{2\pi\sigma_c D}} exp\left[-\frac{1}{2\sigma_c^2} ln^2\left(\frac{D}{D_0}\right)\right] dD \qquad (2)$$

where D is the droplet diameter (mm); D_0 is the mean value of D (mm), and σ_c is the dispersion parameter of the given droplet distribution.

In the PAFOG input script and base parameters, several key elements are integrated across four modules to ensure accurate forecasts; these include the following:

1. Local parameters: geographic information, soil types, vegetation characteristics, and data from weather stations are input to tailor the model to the specific region.
2. Surface data module: it incorporates surface data at the time of forecast calculation, providing real-time inputs for precise predictions.
3. Cloud microphysics module: it addresses cloud cover at low, medium, and high levels, capturing the complex interactions within cloud systems.
4. Radiation calculation module: it uses radiosonde data, air and surface dew point temperatures, and geostrophic wind speed to calculate radiation effects accurately.

Additionally, the fog height parameter in module 1 was adapted to suit the tropical region, ensuring the PAFOG model's applicability and accuracy in the unique climatic conditions of the BNE. Fedorova et al. (2015) found that vegetation parameters did not significantly influence low-visibility forecasts at Maceió Airport. However, humidity from the local lagoon did have an effect (Willett, 1928).

In Modules 2 and 3, observed data from the METAR code were used, whereas in Module 4, ERA5 data were required to fulfill the inputs. Nevertheless, the PAFOG model was employed to predict fog formation at 24-, 18-, 12-, and 6-h intervals in advance. Therefore, it is considered that the forecast product is valid for 6 h.

2.5 Forecast by the FogVIS v.1.0 software

FogVIS is a fog forecasting model developed in the C# programming language using Visual Studio Community. Visibility is calculated using liquid water content (LWC, in g kg^{-1}) and N$_d$ (in cm^{-3}). To estimate the horizontal visibility. The equation proposed by Gultepe and Isaac (2004) was used to calculate N$_d$:

$$N_d = -0.071T^2 + 2.213T + 141.56 \qquad (3)$$

where T refers to the air temperature at the surface, given in ºC.

The LWC for FogVIS is initially estimated using constants and data extracted from the WRF mesoscale model over the BNE, with a script written in the National Center for Atmospheric Research Command Language (NCL; Nobre et al., 2019). However, the PAFOG model generates outputs for the initial hours leading up to the studied case, which, among other results, include LWC values. These initial values were used to match the 24 and 18 h before the occurrence, allowing for a forecast with FogVIS.

As the main goal of this study is to test the applicability of data from diverse sources, it was essential to demonstrate the model's capacity to work effectively with varied datasets. The LWC values generated by PAFOG (Eq. [4]) were then used in FogVIS. The results were consistent with those derived from the method in Nobre et al. (2019), confirming that the LWC approximation performed well within the model framework.

$$LWC = \left(\frac{vis_{data}}{coeff_a}\right)^{\frac{1}{coeff_b}} \bullet \frac{1}{1000} \qquad (4)$$

where vis_{data} is derived from observed data and subsequently processed through the model's parameterization within its modules (non-writable in standard form due to dynamic blocks in Fortran), and $coeff_a$ and $coeff_b$ are coefficients predefined by the type and concentration of parameterized aerosols.

Finally, the calculation of visibility (VIS, in m, Eq. [5]), later proposed by Gultepe et al. (2006), is a function of the two basic variables, N_d (Eq. [3]) and LWC (Eq. [4]), described above.

$$VIS = \frac{1.002}{(LWC \bullet N_d)^{0.6473}} \tag{5}$$

It is important to note that the total number concentration of cloud droplets is denoted as N_c in the PAFOG model and as N_d in the FogVIS algorithm. Despite the difference in notation, both refer to the same physical variable: the total number concentration of cloud droplets (cm^{-3}), as defined by the respective authors of each model.

FogVIS also provides the Fog Stability Index (FSI), an indicator of fog probability based on the atmospheric thermodynamic profile. Developed by the US Air Weather Service in 1979 and refined by Holtslag et al. (2010), the FSI (Eq. [6]) assesses the likelihood of fog or mist occurrence. The index categorizes fog intensity as follows: low (FSI > 55), moderate (31 ≤ FSI ≤ 55), and high (FSI < 31).

$$FSI = 2\left(T - T_d\right) + 2\left(T - T_{850}\right) + W_{850} \tag{6}$$

where T is the air temperature at the surface (ºC), T_d is the dew point temperature (ºC), T_{850} is the air temperature at the level 850 hPa (ºC), and W_{850} is the wind speed at the level 850 hPa (knots).

Horizontal visibility and the FSI were calculated using geographic and meteorological data from the studied airports (Maceió, Recife, and Campina Grande). PAFOG and FogVIS results with METAR data will refine forecasting methods, particularly under extreme conditions. Aligning model predictions with locally observed data is essential for enhancing forecast accuracy in the specific region, the BNE.

2.6 Statistical evaluation

For the statistical evaluation, linear and multiple linear regression techniques were applied to examine the relationships between a weather parameter and visibility during fog events. While qualitative comparisons were made, the study would benefit from a more comprehensive quantitative evaluation.

Applying statistical metrics such as R (Pearson correlation coefficient), R^2 (coefficient of determination), bias, root mean squared error (RMSE), and mean absolute error (MAE) to the entire dataset of fog occurrences would provide a more precise and more robust assessment of model performance, addressing the need for more detailed information on the severe fog events analyzed.

2.6.1 Linear regression

In the linear regression, the observed METAR data were used in relation to the model predictions from PAFOG and FogVIS. The first preliminary step for linear regression involves obtaining a weight K to adjust the model based on the observations. This weight K is given by the variance of the observations and the model, as explicitly shown in Eq. (8):

$$K = \frac{\sigma_{obs}^2}{\sigma_{obs}^2 + \sigma_{model}^2} \leq 1 \tag{8}$$

where σ^2_{obs} is the variance of the observation, and σ^2_{model} the is the model's variance.

It is important to note that $K \approx 1$ corresponds to $\sigma^2_{model} > \sigma^2_{obs}$ and $K \approx 0$ corresponds to $\sigma^2_{model} > \sigma^2_{obs}$. Thus, by obtaining the weight K, it is possible to adjust the model data X_{adj} based on the observations weighted by the variances of the model (σ^2_{model}) and the observations (σ^2_{obs}), as expressed in Eq. (9):

$$Y_{adj} = Y + K(X - Y) \tag{9}$$

where Y_{adj} is the result of the fitted model given the observations; Y is the model prediction, and X is the observed data.

After the model adjustment, linear regression was performed between the observed data (X) and the adjusted model result (Y_{adj}), and statistical metrics were applied, such as R^2, R, bias, RMSE, and MAE, as expressed in the following equations:

$$R = \frac{\sum_{i=1}^{n}(X_i - \bar{X})(Y_i - \bar{Y})}{\sqrt{\sum_{i=1}^{n}(X_i - \bar{X})^2}\sqrt{\sum_{i=1}^{n}(Y_i - \bar{Y})^2}} \tag{10}$$

$$R^2 = (R)^2 \tag{11}$$

$$RMSE = \sqrt{\frac{1}{n}\sum_{i=1}^{n}} \quad (12)$$

$$Bias = \frac{1}{n}\sum_{i=1}^{n}(Y_i - X_i) \quad (13)$$

$$MAE = \frac{1}{n}\sum_{i=1}^{n}\left|Y_i - X_i\right| \quad (14)$$

where X_i are the observed values; $\overline{X}$ is the average of the observed values; Y_i are the adjusted forecast values of the model, and $\overline{Y}$ is the mean of the model's fitted prediction.

2.6.2 Multiple linear regression

For the multiple linear regression, two approaches were used: (1) including METAR data, forecast data, and atmospheric pressure; and (2) using the weight K method, where the model's forecast data were adjusted based on the observations, weighted by the variances of the model (σ^2_{model}) and the observations (σ^2_{obs}). The statistical evaluation was performed using the metrics from Eqs. (10-14).

3. Results and discussion

Across the 13-year period from 2008 to 2020, a total of 218 fog events were documented at the three airports under scrutiny. Notably, 32 events were recorded in SBMO, only one in SBRF, and 185 in SBKG. It is noteworthy that Maceió and Recife are coastal cities, with airport elevations of 108 and 12 masl, respectively, while Campina Grande stands at 502 masl.

The most intense fog cases follow a seasonal pattern, occurring between April and July, aligning with well-established climatological trends for the BNE. This period is heavily influenced by easterly waves that bring moisture from the Atlantic, cooling the region and increasing humidity levels, both conducive to fog formation (Fedorova et al., 2016). Additionally, La Niña years, such as 2017 and 2018, were associated with increased precipitation due to enhanced moisture transport (Molion and Bernardo, 2002), further contributing to fog development in the region.

In terms of modeling, predicting extreme events is relatively difficult. Therefore, the focus is on statistically evaluating the performance and accuracy of the models in forecasting the occurrence of fog and its impact. As a result, the selected cases were characterized by longer duration, lower temperature, severely reduced horizontal visibility, and the presence of other adverse phenomena occurring before, during, and/or after the fog event.

One event from each city (marked in bold letters in Table I) was selected to present the synoptic and thermodynamic patterns in detail. Additionally, the

Table I. Selected intense fog events analyzed in detail.

#	Code	Date/time (UTC)	Duration (h)	Range (m)	Intensity	Adverse phenomena*	Pressure (hPa)
1	SBMO	June 11, 2010/4:00	4:00	200-400	Considerable	BR, FG, BR	1016
2	**SBMO**	**March 07, 2012/8:28**	**2:32**	**0-800**	**Intense**	**FG**	**1015**
3	**SBRF**	**August 18, 2013/15:00**	**1:00**	**700**	**Reasonable**	**RA, FG, RA, BR**	**1017**
4	SBKG	May 03, 2014/9:00	1:00	200	Considerable	BR, RA, FG, RA	1016
5	SBKG	March 21, 2015/3:00	4:00	50-500	Considerable	FG	1012
6	SBKG	February 26, 2016/3:00	3:00	50-700	Intense	FG, BR	1013
7	**SBKG**	**April 02, 2018/3:00**	**1:00**	**500**	**Moderate**	**RA, FG, BR**	**1013**
8	SBKG	April 22, 2018/23:00	1:00	100	Intense	BR, RA, FG	1016
****9a**	**SBMO**	**June 07, 2018/4:25**	**2:35**	**500-700**	**Moderate**	**FG, BR**	**1016**
****9b**	**SBMO**	**June 07, 2018/9:00**	**2:00**	**500-900**	**Reasonable**	**BR, FG, RA**	**1017**
10	SBKG	September 02, 2019/4:00	3:00	200-900	Considerable	BR, FG, RA	1016

SBMO: Maceió International Airport; SBRF: Recife International Airport; SBKG: Campina Grande International Airport; BR: mist; FG: fog; RA: light rain; P: pressure.
*Before/during/after the fog event; **9a and 9b are different events on the same day.
Letters in bold depict an event selected to present detailed synoptic and thermodynamic patterns.
Source: METAR Code.

10 most intense events, which have a significant social impact and greater relevance, were subjected to model evaluation and statistical assessment.

The categorization of fog by Varejão-Silva (2006) was adapted to introduce additional intermediate categories: reasonable (500-700 m) and considerable (100-300 m) between the original light (now 700-1000 m), moderate (now 300-500 m), and intense (now 0-100 m). This modification enables a more nuanced classification of fog events, providing clearer distinctions in intensity and enhancing the statistical analysis in subsection 3.6, thereby facilitating a more precise evaluation of fog forecasting performance. The classification of fog events was based on their maximum development.

3.1 Analysis of fog events in the city of Maceió

Maceió experienced 32 fog instances, primarily in 2008, with June having the highest number of occurrences. Fogs were brief, lasting up to 4 h, and mostly moderate to light, with some instances of low visibility. They typically occurred at dawn or morning, under cloudy skies.

3.1.1 March 07, 2012, an intense event with temperatures above the average

The condition observed from 02:00 to 10:00 UTC, where air temperature (T) and dew point temperature (T_d) were equal ($T = T_d$), meaning the relative humidity was 100%, indicates saturated air at the surface (Fig. 2a), a typical precursor of fog formation. The $T = T_d$ condition caused dew formation during the 6 h before the event, as evidenced by the decreased visibility, which rapidly increased only after the 3-h fog event had occurred.

Satellite and Streamlines observations revealed convective nebulosity in the infrared channel, showing clouds with cold tops and high humidity in the study region (Fig. 2b), induced by a trough (Fig. 2c) from eastern currents associated with a wave disturbance in the trade winds. Although the cumuliform nebulosity expressed a positive convective available potential energy (CAPE; Fig. 2d) above low levels (900 hPa), it is a novel observation that it coexists with fog formation, which requires surface stability.

Therefore, as water vapor condenses into droplets during fog formation, latent heat is released into the surrounding air, stabilizing the temperature and preventing it from continuing to decrease indefinitely. This heat provides a feedback mechanism that counteracts the cooling process, thereby facilitating the maintenance and stabilization of the fog, which can occur both before and after its formation (Houze, 2014).

3.1.2 June 07, 2018, two fog events with mist between them and light rain after

Two fog events occurred on the same day, lasting two and one hour, respectively (Fig. 3a). Surface conditions remained constant with light winds around 6 km h^{-1}. Mist kept visibility low between the events, and light rain reduced visibility for two hours after the second event. Satellite images indicated high pressure at medium levels, with cumuliform clouds observed in the infrared channel (Fig. 3b).

A trough at 1000 hPa showed strong easterly winds diminishing and shifting northwest along the coast (Fig. 3c). The fog was suspended between 975 and 925 hPa due to a humid layer with stable air temperatures and dew points, while the atmosphere remained stable and dry at medium levels (Fig. 3d).

3.2 Analysis of the fog event in the city of Recife

Only one fog event was recorded in Recife during the study period using the METAR code. This occurred on August 18, 2013, and was of mild intensity. Light rain was observed before and during the event, with cloudiness in the vicinity.

Air temperature and dew point were close (around 21-22 ºC), although T and T_d were equal at 08:00 and 10:00 UTC, indicating saturation (100% RH), which does not necessarily indicate fog, since other factors such as radiative cooling, humidity levels, condensation nuclei, and wind conditions are needed for fog formation. Similarly, at 15:00 UTC, when T and T_d differed by 1 ºC, this difference did not prevent fog formation, as additional conditions were met.

Visibility dropped to 700 m at 15:00 UTC, lasting one hour (Fig. 4a). Infrared imagery showed warm top cloudiness without a frontal system (Fig. 4b). A decaying trough influenced the region (Fig. 4c). High humidity and fog were near the surface, with an altostratus layer up to 600 hPa. The atmosphere was stable and humid to mid-levels (Fig. 4d).

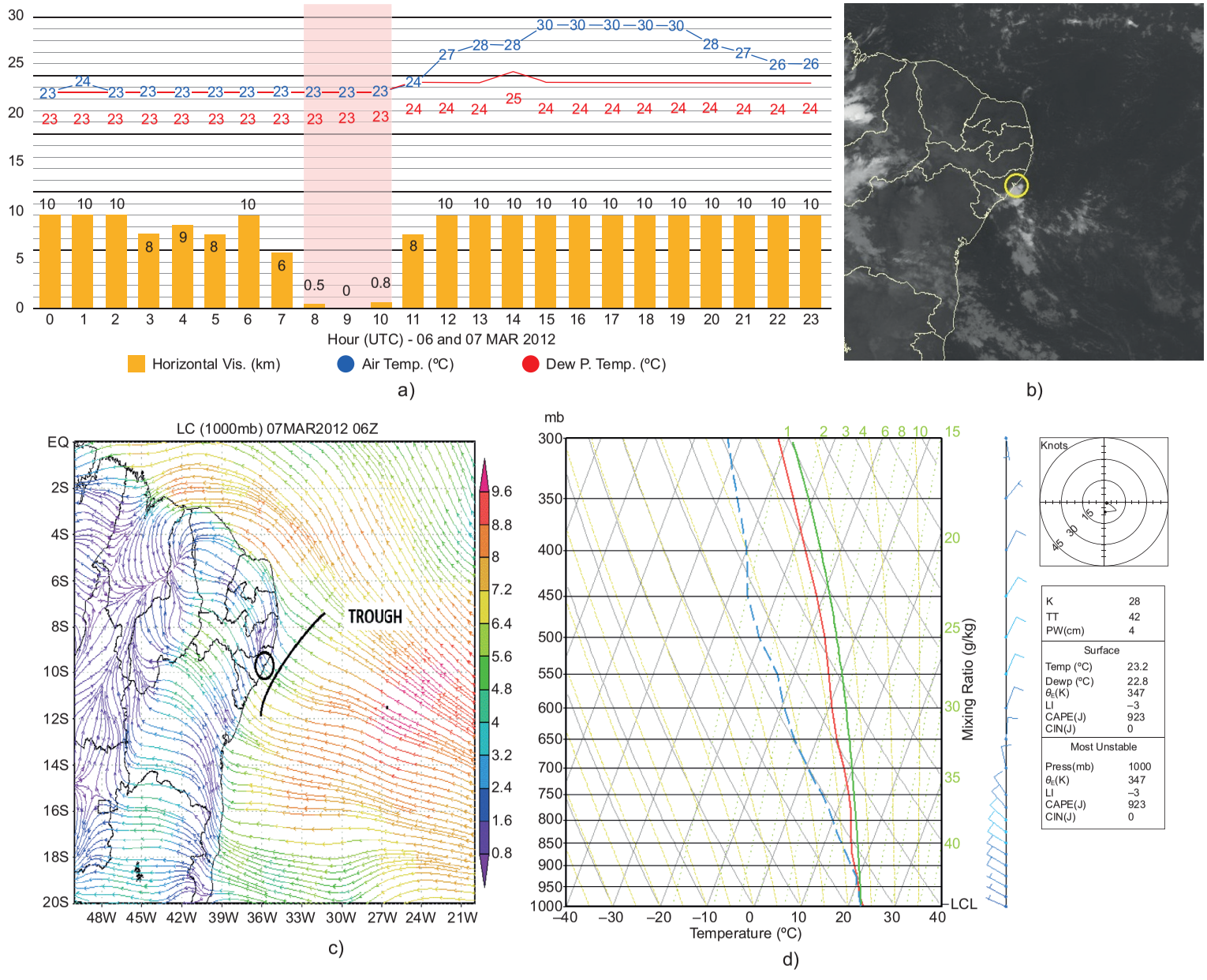

Fig. 2. Synoptic and thermodynamic fields for March 07, 2012. (a) Surface data; (b) satellite images (infrared); (c) streamlines at 1000 hPa, and (d) Skew-T/Log-P. Source: METAR code, CPTEC, ERA5.

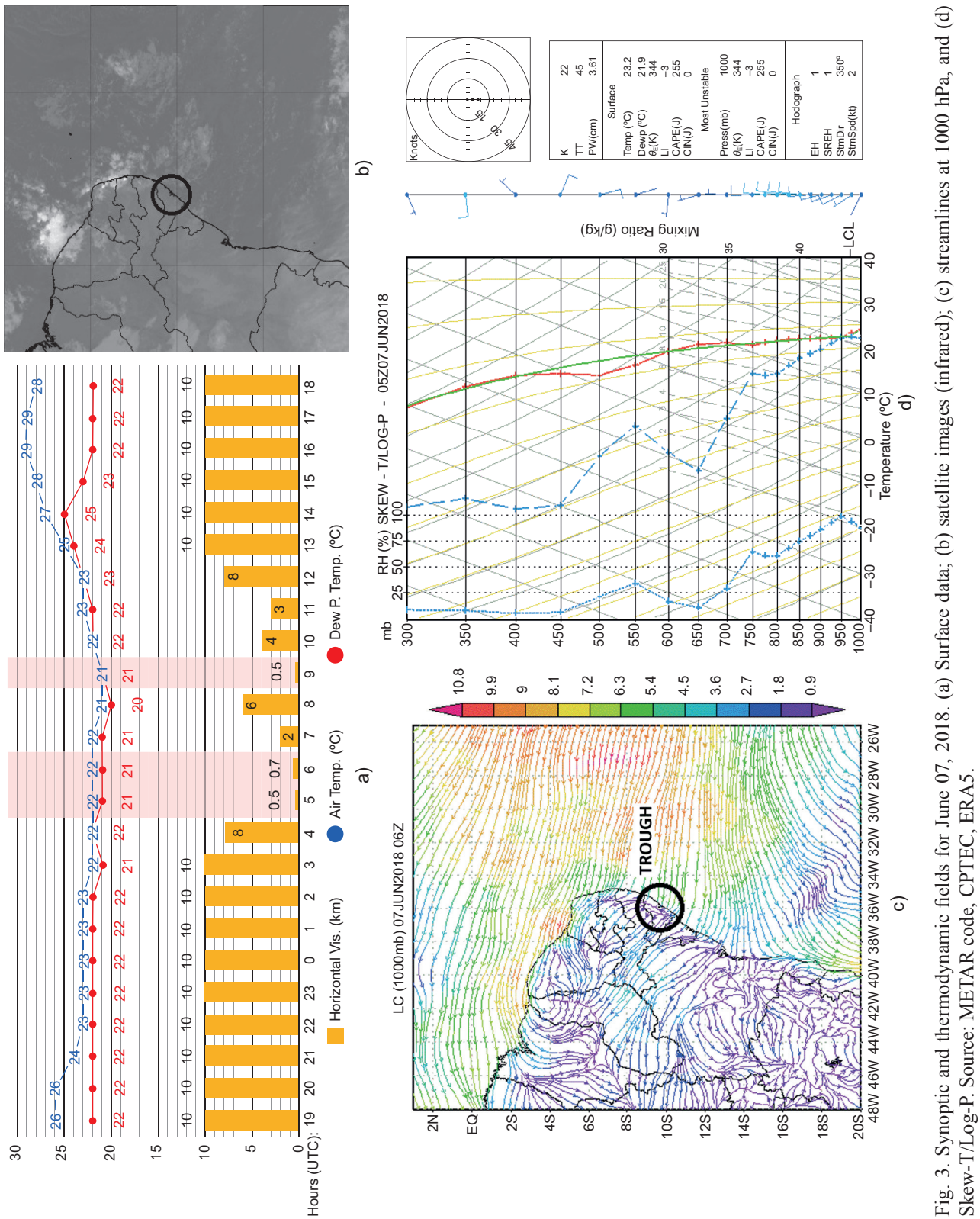

Fig. 3. Synoptic and thermodynamic fields for June 07, 2018. (a) Surface data; (b) satellite images (infrared); (c) streamlines at 1000 hPa, and (d) Skew-T/Log-P. Source: METAR code, CPTEC, ERA5.

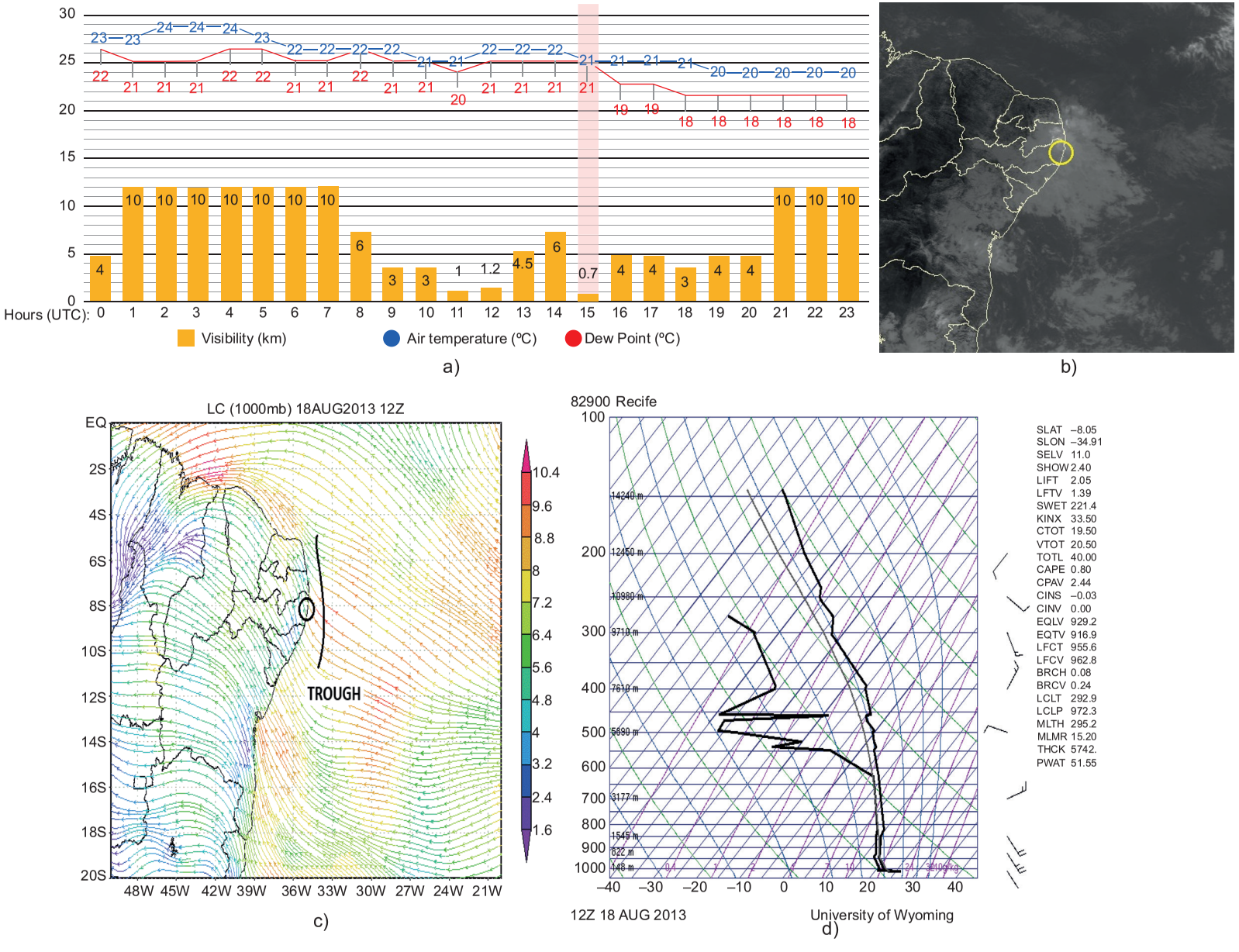

Fig. 4. Synoptic and thermodynamic fields for August 18, 2013.(a) Surface data; (b) satellite images (infrared); (c) streamlines at 1000 hPa, and (d) Skew-T/Log-P. Source: METAR code, CPTEC, ERA5.

3.3 Analysis of fog events in the city of Campina Grande

A total of 185 fog events were recorded at Presidente João Suassuna airport in Campina Grande using the METAR code. Most of it occurred between May and July, coinciding with the region's rainy season in autumn and winter. The highest occurrences were in 2013 and 2018, with only one recorded in 2010. The fog events reached maximum intensity quickly but were short-lived. Of the 185 events, 32 were intense, 95 moderate, and 58 light, with an average duration of 90 min.

On April 2, 2018, a fog event occurred, preceded by light rain and followed by mist. From 02:00 to 09:00 UTC, $T = T_d$ indicated air saturation, but this alone did not lead to fog formation, as explained in subsection 3.2. The saturation was likely caused by moisture transport from the reservoir, with low wind speed further enhancing fog development. Despite $T = T_d$ during the entire period, the conditions for fog formation were only met at 03:00 and 04:00 UTC, when these factors aligned to increase droplet concentration and reduce visibility.

This allowed the fog to develop rapidly and dissipate gradually, maintaining 100% humidity for an extended period. While $T = T_d$ marks air saturation, fog formation also depends on radiative cooling, high humidity, condensation nuclei, and local weather conditions. The METAR code indicated light rain followed by moderate rainfall and significant cloudiness, suggesting that thermal inversion trapped moisture near the surface, facilitating fog formation. This period lasted from 02:00 to 09:00 UTC (Fig. 5a). During the event, wind speeds decreased from 12 to 5 km h^{-1}. The water vapor channel of satellite imagery (Fig. 5b) shows a moisture gradient, with medium to high levels over the northern coast and dry conditions in the hinterland.

Near the surface (1000 hPa), there is a confluence of cyclones and anticyclones affecting the city. At medium levels (600 hPa), a weak trough is present (Fig. 5c). The region experiences a confluence of two trough currents with a ridge from the Southern Hemisphere, indicating strong descending movements. This likely contributes to the dry air mass, inhibiting cloud formation at medium levels. With the thermodynamic diagram (Fig. 5d), it is also possible to observe a very thick wet layer between 1000 and 800 hPa.

3.4 Fog forecast by the PAFOG model

3.4.1 Maceió

On March 07, 2012, the PAFOG model did not predict fog (values below 1000 m; Fig. 6a), although it did calculate a reduction in horizontal visibility during the event. For the double event on June 07, 2018, all calculations were interrupted despite the height adjustment (Fig. 6b). Two events occurred, so calculations were labeled A, B, C, and D, initiated at 6-h intervals. Forecast A predicted fog lasting 2 h; forecast B predicted fog earlier than observed; calculation C predicted both fogs but at different times, and forecast D predicted the second fog at the observed time but with a longer duration.

3.4.2 Recife

On August 18, 2013, the PAFOG model performed very satisfactorily. Fog was predicted in all calculations, though interruptions occurred in each (Fig. 6c). The 24-h antecedence forecast predicted two fog events, one long and one short. The 18 and 12-h forecasts predicted fog at the correct time. The 6-h antecedence forecast predicted a short fog that formed 1 h before the observed time.

3.4.3 Campina Grande

On April 02, 2018, there was a reduction in horizontal visibility just one hour before the event (Fig. 6d). The PAFOG model's 24-h antecedence forecast predicted two periods of fog. The 18-h forecast predicted three periods of fog, while the 12 and 6-h forecasts each predicted one period of fog. The 24 and 18-h forecasts indicated longer fog durations than observed, but at different times. However, the 12- and 6-h forecasts showed visibility gradually decreasing and accurately reported fog at the time recorded by METAR.

3.5 Fog forecast by the FogVIS software

The results of the comparison are presented in Table II. For some events, PAFOG was unable to predict fog (< 1000 m). In these cases, the model interpreted the event as mist (> 1000 m). However, in general, FogVIS indicated good fog stability: weak with 24 h antecedence and moderate with 18 h antecedence.

The FSI indicates the likelihood of fog formation and proved more efficient when the observed fog had a short horizontal visibility range from formation to dissipation. When FSI indicated a low probability

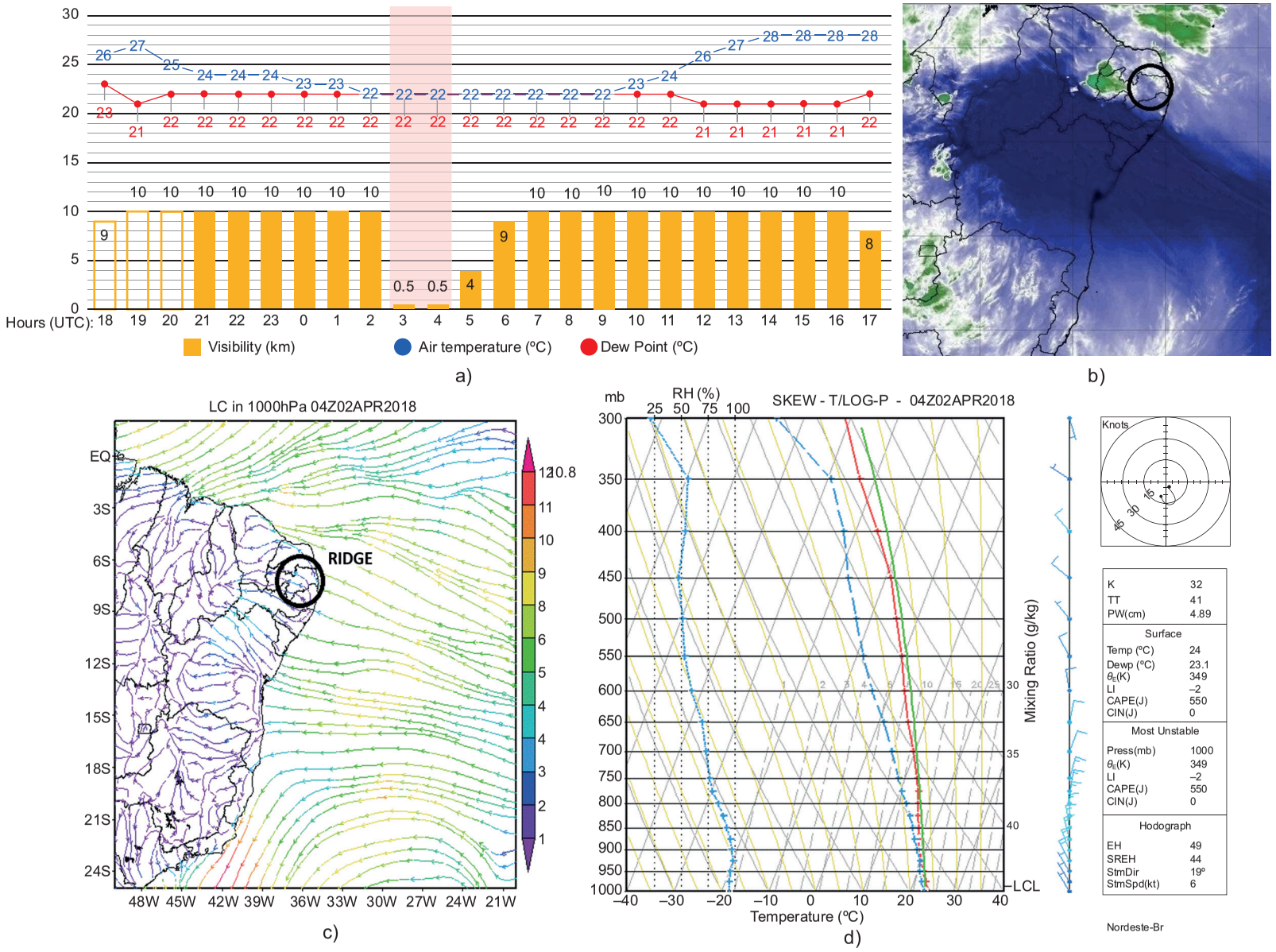

Fig. 5. Synoptic and thermodynamic fields for April 02, 2018.(a) Surface data; (b) satellite images (infrared); (c) streamlines at 1000 hPa, and (d) Skew-T/Log-P. Source: METAR code, CPTEC, ERA5.

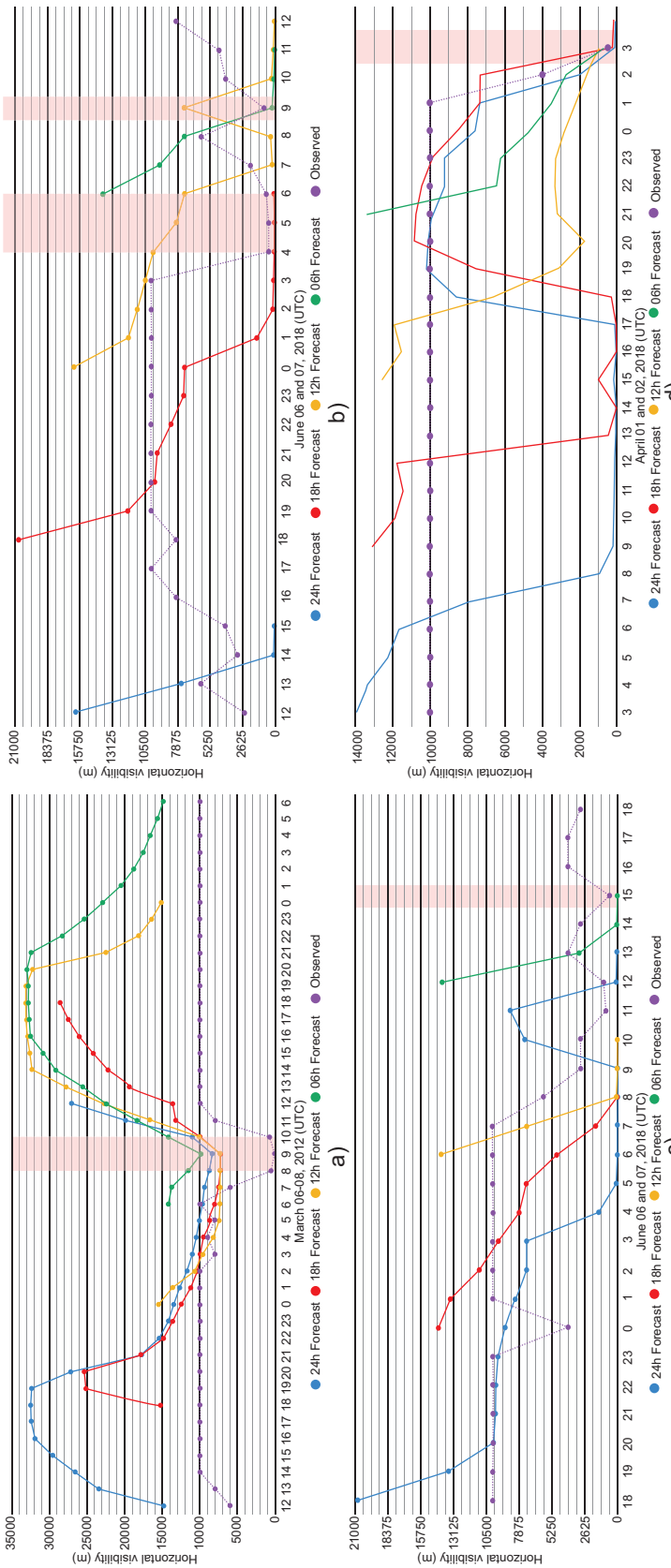

Fig. 6. Fog forecast by the PAFOG model.

Table II. Comparison of METAR code, PAFOG, and FogVIS forecasting.

#	METAR (m)	PAFOG horizontal visibility (m)				FogVIS horizontal visibility (m)		FogVIS Fog Stability Index	
	Initial	24 h	18 h	12 h	6 h	24 h	18 h	24 h	18 h
1	400	1000	50	50	1000	598.1	308.8	60.0 (low)	42.8 (moderate)
2	**500**	**1000**	**1000**	**1000**	**1000**	**165.7**	**216.6**	**42.2 (moderate)**	**48.7 (moderate)**
3	**700**	**840**	**526**	**497**	**288**	**239.9**	**281.0**	**38.9 (moderate)**	**43.1 (moderate)**
4	200	1000	271	159.2	296	429.5	527.8	48.1 (moderate)	71.1 (low)
5	500	1000	219.4	1000	250	643.6	365.9	44.5 (moderate)	54.0 (moderate)
6	700	941.1	122	1000	1000	566.5	387.7	42.5 (moderate)	46.5 (moderate)
7	**500**	**960**	**481**	**927**	**720**	**919.8**	**399.7**	**19.6 (high)**	**20.6 (high)**
8	100	172	362	57	48	797.1	440.3	30.2 (high)	19.1 (high)
9a	**500**	**92.2**	**182**	**374**	**240**	**554.8**	**413.3**	**32.7 (moderate)**	**37.8 (moderate)**
9b	**500**	**65**	**105**	**281**	**89**	**704.8**	**513.3**	**32.7 (moderate)**	**37.8 (moderate)**
10	900	323.6	79.5	1000	1000	310.0	968.1	55.7 (low)	53.2 (moderate)

Rows in bold letters represent the events shown in Figures 2-5.

of fog formation, PAFOG and FogVIS made highly accurate predictions, with results within the observed range. FogVIS horizontal visibility prediction calculations and FSI were most efficient at 18 h antecedence, indicating a high possibility of fog occurrence and more accurate intensity forecasts.

3.6 Statistical evaluation

In shorter forecast timeframes (12 h [Fig. 7c] and 6 h [Fig. 7d]), PAFOG shows relatively significant results in its predictive ability. In the 12 h forecast, $R^2 = 0.92$ and $R = 0.96$ were obtained, indicating that more than 90% of the observed variance is explained by the adjusted model. The moderate bias (17.49 m) and RMSE = 69.10 m attest to reduced absolute errors.

In the 06 h forecast, $R^2 = 0.98$ and $R = 0.94$ were obtained, with almost zero bias (9.23 m) and RMSE = 79.10 m, reaffirming the statistical significance of the short-term adjustment.

For longer periods (24 h [Fig. 7a] and 18 h [Fig. 1b]), the adjustment loses some of its effectiveness. In the 24-h forecast, $R^2 = 0.78$ and $R = 0.88$ are observed, which, although still satisfactory, reveal greater dispersion of points between METAR and PAFOG. The bias of 39.31 m and RMSE = 108.46 m suggest systematic overestimation, and the positive intercept (approximately 150 m) reinforces this shift, as expressed in the identity equation. In the 18-h forecast, values of $R^2 = 0.57$ and $R = 0.75$ indicate moderate statistical performance, with a negative bias (–74.71 m), showing a tendency for underestimation and RMSE = 159.03 m.

Among the positive aspects of PAFOG model, the K-weight method highlights the variability of the model in relation to the observations, significantly increasing the correlation in the 6-12-h horizons. The main limitations were observed in the 18-24-h forecasts, where bias persists and RMSE increases, demonstrating that the simple linear adjustment does not fully capture physical processes and potential nonlinearities in longer forecast horizons.

Regarding the FogVIS prediction, in the 24-h forecast (Fig. 7e) there is a soft linear adjustment, with $R^2 = 0.32$ and $R = 0.57$. The high RMSE (176.74 m) and MAE = 150.34 m indicate substantial errors.

In the 18-h forecast (Fig. 7f), there is moderate improvement, with $R^2 = 0.64$ and $R = 0.80$, however still inferior to PAFOG. The bias of –34.44 m and RMSE = 133.20 m suggest underestimation in some cases.

As for FogVIS, its limitations are evident, as it exhibits high error and low explanatory power in the 24-h prediction, possibly due to simplifications in the physical scheme or the lack of additional meteorological variables in the adjustment. Its performance within the 18-h forecast shows better predictive skill, as indicated by the statistical metrics. It is important to note that the published results for FogVIS were

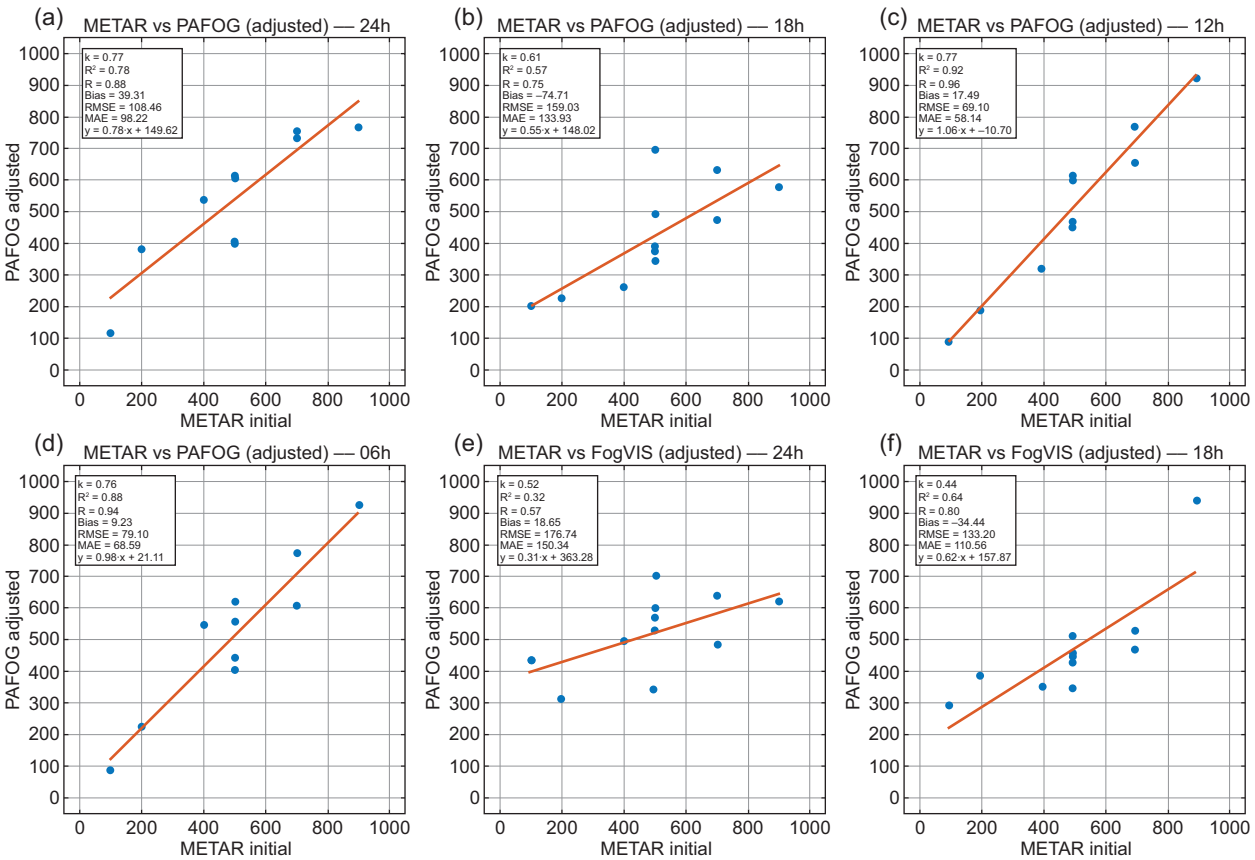

Fig. 7. Statistical evaluation of severe fog events after mathematical adjustments. Source: METAR code, ERA5, PAFOG, FogVIS.

originally only for 24-h forecasts. In this study, the 18-h forecast was tested as an alternative, and the results demonstrated improved performance.

For the results of the multiple linear regression, including atmospheric pressure and weight K (Table III), it is evident that PAFOG correlations are statistically significant in the short-term forecast horizons. In the 6-h forecast, it is possible to explain 88% of the observed variance with almost zero bias (9.23 m) and an RMSE of only 23.15 m. In the 12-h forecast, $R^2 = 0.98$ was obtained, with RMSE around 58.65 m. For longer periods (18 and 24 h), although still statistically significant, the performance decreases (R^2 of 0.57 and 0.84, respectively), RMSE increases above 100 m, and systematic biases appear, with underestimation at 18 h and overestimation at 24 h.

In the case of FogVIS, the adjusted correlation remains only moderate ($R \approx 0.81$ at 18h) and it decreases significantly at 24 h ($R^2 \approx 0.45$), with RMSE exceeding 150 m and alternating positive and negative biases. This performance suggests that the original physical scheme of FogVIS, even when weighted by the K weight and atmospheric pressure, possibly lacks additional variables such as humidity or temperature.

4. Conclusion

Over a 13-year period, 218 fog events were identified across three BNE airports. Fog occurrences in all cities were concentrated between April and August, the local rainy season, and were linked to southeast-originating air masses, with surface evaporation from the ocean and lagoon, supported by a wet layer close to the surface, serving as a key humidity source.

The most intense and prolonged fog events for each city followed consistent patterns, as demonstrat-

Table III. Historical statistical evaluation of the severe fog events analyzed using the PAFOG and FogVIS models.

Model	Lead time (h)	k	R^2	R	Bias	RMSE	MAE	Equation
PAFOG	24 h	0.77	0.84	0.92	39.31	77.54	68.036	$\hat{y} = 0.76 \cdot METAR - 29.09 \cdot P + 29693.50$
PAFOG	18 h	0.61	0.57	0.75	-74.71	121.05	103.37	$\hat{y} = 0.55 \cdot METAR - 4.42 \cdot P + 4634.51$
PAFOG	12 h	0.77	0.98	0.99	17.49	58.65	43.709	$\hat{y} = 1.03 \cdot METAR - 33.49 \cdot P + 34001.64$
PAFOG	06 h	0.76	0.88	0.95	9.235	23.15	18.318	$\hat{y} = 0.97 \cdot METAR - 12.63 \cdot P + 12845.64$
FogVIS	24 h	0.52	0.45	0.67	18.65	153.97	119.4	$\hat{y} = 0.29 \cdot METAR - 25.72 \cdot P + 26489.10$
FogVIS	18 h	0.44	0.66	0.81	-34.44	92.54	76.765	$\hat{y} = 0.63 \cdot METAR + 15.65 \cdot P - 15738.74$

k: weighting factor; R^2: coefficient of determination; R: Pearson correlation coefficient; RMSE: root mean squared error; MAE: mean absolute error.
Source: METAR code, ERA5, PAFOG, FogVIS.

ed in the detailed examples presented in the results section. These patterns were verified through the analysis of surface data, satellite imagery, streamlines, and thermodynamic diagrams. Therefore, if similar conditions for severe fog formation are present in other periods or cities, the results are expected to align closely with those observed. If these conditions are only partially met or not met at all, the fog events will be less severe, shorter in duration, and with significantly reduced social impact, or potentially insignificant. These conditions in each city are detailed next.

In Maceió (32 events) and Recife (one event), fog was occasionally followed by mist or light rain, enhancing air humidification, and was associated with a low-level trough (low pressure on the surface) and a mid-level ridge, creating a humidity-trapping configuration. Half of the cases in Maceió (M) occurred under clear skies before mist formation, indicative of radiation fog. The rarity of fog in Recife (R) underscores its atypical conditions for fog development.

In Campina Grande (185 events), fog was intense, marked by convective cloud cover and high surface humidity. Atmospheric conditions featured a ridge at 1000-850 hPa (high pressure on the surface) and mid-level troughs, promoting lifting at 900 hPa and inhibiting mid-level cloud formation. These are characteristic features of the advection fog, in contrast to the coastal cities of Maceió and Recife.

Thermodynamic analyses showed air lifting and moistening in the 1000-850 hPa layer across events; however, terminal aerodrome forecasts (TAFs) did not anticipate visibility reductions below 1000 m. PAFOG's performance varied by location, demonstrating high accuracy in Maceió, particularly when adverse weather followed fog events. However, in Campina Grande, PAFOG occasionally mistimed the onset of fog under specific conditions. In contrast, FogVIS performed better in Campina Grande, especially for events with minimal variation in the observed horizontal visibility range.

Both models demonstrated efficiency, with PAFOG excelling in Maceió and FogVIS in Campina Grande. The PAFOG model showed particularly strong predictive performance in shorter forecast horizons. The 12- and 6-h forecasts show a close alignment with METAR observations, with the 12-h forecast being especially accurate. FogVIS did not perform as well, although its 18-h forecast showed better results than the 24-h forecast.

A comparative analysis between the two models clearly indicates that PAFOG outperforms FogVIS, particularly in extreme fog cases. This is consistent across both linear and multiple linear regression evaluations, where PAFOG consistently demonstrates superior accuracy in predicting severe fog events, reinforcing its reliability for operational use in the BN.

Acknowledgments
A special thanks to Prof. Andreas Bott, Meteorological Institute, University of Bonn, Germany, for providing the PAFOG model. We are grateful for the

financial support provided by the Federal University of Alagoas (UFAL) and the National Council of Scientific and Technological Development (CNPq) as student grants.

References

Akimoto Y, Kusaka H. 2015. A climatological study of fog in Japan based on event data. Atmospheric Research 151: 200-211. https://doi.org/10.1016/j.atmosres.2014.06.001

Bott A, Trautmann T. 2002. PAFOG – A new efficient forecast model of radiation fog and low-level stratiform clouds. Atmospheric Research 64: 191-203. https://doi.org/10.1016/S0169-8095(02)00091-1

Chaumerliac N, Richard E, Pinty JP, Nickerson EC. 1987. Sulfur scavenging in a mesoscale model with quasi-spectral microphysics: Two-dimensional results for continental and maritime clouds. Journal of Geophysical Research 92: 3114-3126. https://doi.org/10.1029/JD092iD03p03114

Cotton WR, Anthes RA. 1989. Storm and cloud dynamics. Academic Press, San Diego, New York, Berkeley, Boston, London, Sydney, Tokyo, Toronto, 883 pp.

Fedorova N, Levit V, de Souza JL, Silva AO, Afonso JMS, Teodoro I. 2015. Fog events at Maceio airport on the northern coast of Brazil during 2002-2005 and 2007. Pure and Applied Geophysics 172: 2727-2749. https://doi.org/10.1007/s00024-014-1027-0

Fedorova N, Levit V. 2016. Fog in the tropical region: Fog formation in the tropical region of the northeast of Brazil. Lap Lambert Academic Publishing, Saarbrücken, Germany, 82 pp.

França GB, de Carmo LFR, de Almeida MV, Albuquerque-Neto FL. 2019. Fog at the Guarulhos international airport from 1951 to 2015. Pure and Applied Geophysics 176: 2191-2202. https://doi.org/10.1007/s00024-018-1781-5

Gultepe I, Isaac GA. 2004. Aircraft observations of cloud droplet number concentration: Implications for climate studies. Quarterly Journal of the Royal Meteorological Society 130: 2377-2390. https://doi.org/10.1256/qj.03.120

Gultepe I, Müller MD, Boybeyi Z. 2006. A new visibility parameterization for warm-fog applications in numerical weather prediction models. Journal of Applied Meteorology and Climatology 45: 1469-1480. https://doi.org/10.1175/JAM2423.1

Houze RA Jr. 2014. Cloud dynamics. Academic Press, Oxford, UK, 432 pp.

Holtslag MC, Steeneveld GJ, Holtslag AAM. 2010. Fog forecasting: "Old fashioned" semi-empirical methods from radio sounding observations versus "modern" numerical models. In: Proceedings of the 5th International Conference on Fog, Fog Collection and Dew. Münster, Germany, 1-4.

Lawrence MG. 2005. The relationship between relative humidity and the dewpoint temperature in moist air: A simple conversion and applications. Bulletin of the American Meteorological Society 86: 225-233. http://doi.org/10.1175/BAMS-86-2-225

Melo DL, Oliveira CG, Fedorova N, Levit V. 2023. Fog analysis and forecast by PAFOG model in Brazilian northeast. Revista Brasileira de Meteorologia 38: e38230215. https://doi.org/10.1590/0102-77863810215

Molion LCB, Bernardo SO. 2002. Uma revisão da dinâmica das chuvas no nordeste brasileiro. Revista Brasileira de Meteorologia 17:1-10.

Nickerson EC, Richard E, Rosset R, Smith DR. 1986. The numerical simulation of clouds, rains and airflow over the Vosges and Black Forest Mountains: A Meso-β model with parameterized microphysics. Monthly Weather Review 114: 398-414. https://doi.org/10.1175/1520-0493(1986)114<0398:TNSOCR>2.0.CO;2

Nobre JPG, Fedorova N, Levit V, Dos Santos AS, Lyra MJA. 2019. Nova metodologia para previsão de eventos de nevoeiro para o Aeroporto Zumbi dos Palmares em Maceió (Alagoas). Anuário do Instituto de Geociências 42: 527-535. https://doi.org/10.11137/2019_3_527_535

Varejão-Silva MA. 2006. Meteorologia e climatologia. Recife, Brazil, 463 pp. Available at: chrome-extension://efaidnbmnnnibpcajpcglclefindmkaj/https://icat.ufal.br/laboratorio/clima/data/uploads/pdf/METEOROLOGIA_E_CLIMATOLOGIA_VD2_Mar_2006.pdf

Willet HC. 1928. Fog and haze, their causes, distribution and forecasting. Monthly Weather Review 56: 435-468. https://doi.org/10.1175/1520-0493(1928)56<435:FAHTCD>2.0.CO;2